Available online at www.sciencedirect.com

ScienceDirect

Physics Procedia 56 (2014) 411 – 420

Physics Procedia

8th International Conference on Photonic Technologies LANE 2014

Mathematical modeling of crystal growth and microstructure formation in multi-layer and multi-track laser powder deposition of single-crystal superalloy

Zhaoyang Liu[a,]*, Huan Qi[a]

[a]*University of Michigan – Shanghai Jiaotong University Joint Institute, 800 Dongchuan Road, Shanghai, 200240, China*

Abstract

A self-consistent three-dimensional mathematical model was developed to predict the crystal growth and microstructure formation in multi-layer and multi-track laser powder deposition of single-crystal superalloy. Laser powder deposition experiments with nickel-based single-crystal superalloy were conducted to verify the computational results. The results indicated that the overlapping ratio was the key parameter to ensure the continuity and consistency of the epitaxial columnar dendrite growth. Both small and large overlapping ratios lead to residual stray grain region of the previously deposited layer. Scanning with alternating X and Y direction method produces better result with the continuous columnar dendrite growth compared to that of the one direction scanning method. With proper deposition parameters and the alternating scanning method, the epitaxial growth of columnar dendrite microstructure can be achieved in a multi-track and multi-layer deposit.

© 2014 Published by Elsevier B.V. This is an open access article under the CC BY-NC-ND license (http://creativecommons.org/licenses/by-nc-nd/3.0/).
Peer-review under responsibility of the Bayerisches Laserzentrum GmbH

Keywords: multi-layer and multi-track; laser powder deposition; single-crystal; microstructure

* Corresponding author. Tel.: +86-13917252514 ; fax: +86-21-34206525 .
E-mail address: zhaoyang_liu8585@163.com

1875-3892 © 2014 Published by Elsevier B.V. This is an open access article under the CC BY-NC-ND license (http://creativecommons.org/licenses/by-nc-nd/3.0/).
Peer-review under responsibility of the Bayerisches Laserzentrum GmbH
doi:10.1016/j.phpro.2014.08.144

1. Introduction

Single-crystal (SX) nickel-based superalloys have been used in aircraft and land-based turbine energy systems over the last 20 years[1, 2]. The elimination of the constituents needed for grain boundary strengthening improves the high-temperature creep resistance and thermal fatigue behaviour of SX nickel-based superalloys. Hence the operating temperature of SX turbine blade can be increased, which improves the associated efficiency and performance of gas turbines[3]. Until now, casting technology is the main method to manufacture the SX turbine blade with an accurate control of temperature gradient and crystal orientation in mode. Nevertheless casting technology has some disadvantages such as high failure rate, casting defects, long production cycle, high cost, etc., which greatly increases the price of SX turbine blade and associated maintenance cost of modern gas turbines. At present, LPD technology, as a very useful repair technology, has been used to restore the casting defects or worn squealer tips of casting SX turbine blade in a near-net-shape way. Many researchers have shown that due to the high temperature gradient (>10^6 K/m) of LPD processing and epitaxial growth characteristic of SX superalloy, the small columnar dendrite grows epitaixally from the partial melted substrate and therefore in the repair zone, the SX solidification microstructure can be achieved identical to SX substrate[4]. Moreover, LPD technology can manufacture dense parts of various kinds of material line by line and layer by layer with CAD, CAM and monitoring and feedback control methods. The same technology is also called by other names, i.e. Direct Metal Deposition (DMD)[5], Direct Laser forming (DLF)[6] or Laser metal forming (LMF)[7]. This manufacturing method has no constraints on part shape and powder material relative to traditional manufacturing methods such as casting and forging. Gaumann et al.[8] coupled the epitaxial growth characteristic of SX superalloy and LMF technology to develop a process of epitaxial laser metal forming (E-LMF). This process showed that the fined epitaxial columnar dendrite can be achieved in multilayer LPD of SX superalloy and provide a way to control the microstructure in parts. Due to the characteristic of rapid prototyping and near-net-shape, E-LMF process provides a method to manufacture SX turbine blade with low cost. Recently, some preliminary researches have shown that the continuous columnar dendrite could be achieved in the multilayer and multi-track DMD processing of directional solidified alloy DZ125[9]. Thus further study of the crystal growth and microstructure formation in multi-layer and multi-track LPD of SX superalloy is valuable for the development of E-LMF process and the manufacture of SX turbine blades.

Currently, there still are many drawbacks need to be solved in the LPD processing of SX superalloy. The major one is stray grains which appear as misoriented grain defects in the SX solidification[2]. Stray grains, once form, remove the desirable SX microstructure and, furthermore, cause low melting grain boundaries acting as easy path for crack initiation and propagation. Thus nickel-based SX superalloys are vulnerable to the stray grain formation. Many researchers have studied the mechanism of stray grain formation by mathematical models [8, 10-15] and experimental approaches[16, 17]. The results show that the mechanism of stray grain formation is equiaxed grain nucleation and growth ahead of the solidification interface when the extent of constitutional supercooling (CS) is enough. Hunt[10] initially showed that the CS can be described by the G/V ratio, where G is the thermal gradient and V is solidification velocity. Gaumman et al.[4] developed hunt's[10] morphological transition of growing dendrites model, and derived a simplified analysis applicable to complex multi-component alloy systems. It was demonstrated that a fully columnar structure can be obtained when the ratio G^n/V exceeds a critical value (G is the temperature gradient, V is the solidification velocity and n is a material-dependent constant). Low temperature of substrate, low laser power and small laser beam diameter could advance the continuously epitaxial growth of columnar dendrite in multi-layer LPD processing. Similarly, Rappaz et al.[11, 12] and Liu et al.[13, 14] used smallest growth velocity criterion to describe the crystal growth pattern. Their work contributes to the understanding of effects of the molten pool shape and substrate crystallographic orientation on the microstructure formation in molten pool. Recently, Anderson et al.[15] combined a heat transfer and fluid flow model and Gaumann's[8] columnar-to-equiaxed transition (CET) model to analyze the effect of processing parameters on stray grain formation. This work provides a way to use transient mathematical model to study the molten pool shape and associated crystal growth.

All these findings have contributed to the understanding of the crystal growth and microstructure formation during sing-track laser surface remelting or LPD processing. The crystal growth and microstructure formation in deposited bead can be well predicted and controlled by designed molten pool geometry and substrate crystallographic orientation. Unlike single-track deposition, the materials in each track will undergo successive thermal cycles as the laser beam moves to the other tracks in multi-layer and multi-track LPD processing. The processing parameters (diameter and spatial distribution of laser beam and powder flow), heat-transfer conditions

and underlying crystallographic orientation for epitaxial growth vary due to the overlap of multi deposited bead.

In this study, a 3D transient numerical model was developed to simulate the crystal growth and microstructure formation in multi-layer and multi-track LPD processing of SX superalloy. LPD experiments with SX alloy Rene N5 were conducted to verify the computational results of microstructure in deposited bead. The effects of overlapping ratio (OR) and scanning method on crystal growth and microstructure formation were studied through the mathematical modeling and experimental results.

2. Mathematical model

2.1. 3D Mathematical model of transport phenomena

In the past decade, many mathematical models have been developed to study the transport phenomena of LPD processing [18-26]. Until now, the most recent and complete 3D mathematical model of transport phenomena during single-layer or multi-layer LPD processing of SX superalloy is that of Liu et al.[27]. Liu's 3D mathematical model can accurately calculate the deposited bead geometry, temperature field, and fluid flow and associated dynamic molten pool shape. In this model, Liu's 3D mathematical model in previous work [27] and a new established crystal growth model is coupled to build an advanced and complex simulation model for crystal growth in the deposited bead. The detailed description of transport phenomena portion in the 3D mathematical model can refer to Liu's previous work [27]. A schematic of the 3D coaxial LPD process in the study is shown in Fig. 1. In this physical model, the position of substrate is stationary in a 3D Cartesian coordinate with the (001)/[100] crystallographic orientation normal to the top surface. A focused laser beam is striking on the substrate and scanning along the positive X direction ((100)/[001] crystallographic orientation) at a constant speed V_b. Metal powder is delivered through gas flow coaxially with the laser beam and interacts with laser beam. A deposited layer is formed as a result of continuous melting of captured powder and solidification of molten pool with the moving laser beam. The melts solidify very quickly due to the associated high cooling rate. A laser beam with a Gaussian profile is used as the heat source, which is focused on the substrate surface with a spot size of 0.6 mm at a distance of 9 mm below the nozzle tip.

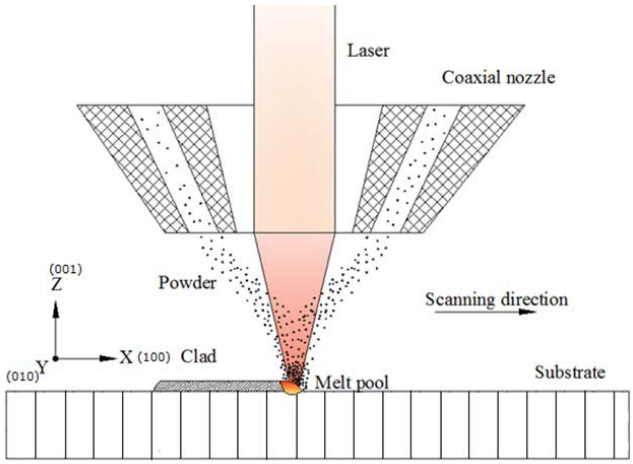

Fig. 1. A schematic of the coaxial laser powder deposition process.

2.2. Crystal growth model

In the above coaxial LPD processing, the transient evolution the molten pool shape corresponds to the temperature field and is updated at every time step in the simulation. Based on the temperature field and dynamic molten pool shape calculated from the above 3D mathematical model, the crystal growth and microstructure formation in the molten pool can be predicted by an established crystal growth model. Figure 2 shows the geometric relationship of variables used in the following derivation of crystal growth model.

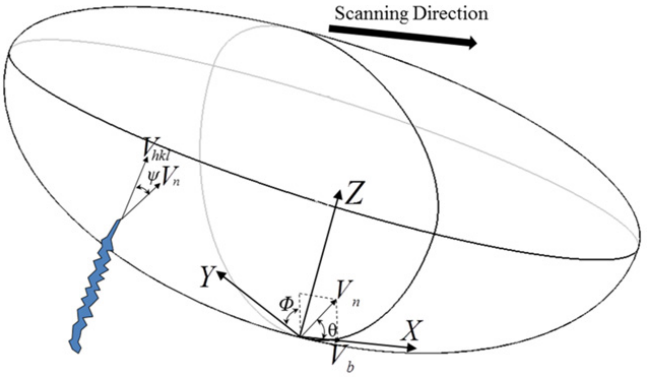

Fig. 2. Schemetic representation of 3D molten pool shape with dynamic local coordinate system.

The crystal growth and microstructure formation in molten pool responds to the solidification conditions ahead of the advancing solidification interface[10]. The criterion which states the microstructure is columnar dendrite can be derived when the following condition is satisfied everywhere in the molten pool[4]:

$$\frac{G^n}{V} > K_{CET} = a\left\{\sqrt[3]{\frac{-4\pi N_0}{3In(1-\phi_c)}}\frac{1}{n+1}\right\}^n \tag{1}$$

where G is the temperature gradient, V is the solidification velocity of the columnar dendrite tip and K_{CET} is the critical value of CET. The a and n are material dependent parameters, and N_0 is the nucleation density in the liquid. A parameter φ_c was defined as the critical value of areal fraction ahead of the advancing solidification front that is comprised of newly nucleated grains.

Gaumann et al.[4] used the alloy CMSX 4 in his work and it is assumed that the material parameters used in equation (1) are generally applicable to the entire class of SX nickel-based superlloys. Vitek et al.[28] and Liu et al.[29] used material parameters of CMSX-4 in their model, and had shown that the simulation result can also analyse the crystal growth and microstructure formation of Rene N5. The nominal composition of the Rene N5 alloy is Ni-8Co-7Cr-6.2Al-5W-6Ta-3Re-2Mo-0.1Hf (in wt. %) while the CMSX-4 alloy has a similar composition of Ni-9Co-6.5Cr-5.6Al-1Ti-6W-6.5Ta-3Re-0.6Mo-0.1Hf (in wt. %). In this study, Rene N5 was used as depositing material, and the material parameters a, n, φ_c and N_0 in the mathematical model are also taken the same values as used for CMSX 4 in the model of Gaumann et al.[4] which means $a = 1.25\times10^6$ $K^{3.4}/m$ s, $n = 3.4$, $\varphi_c = 0.0066$ and $N_0 = 2\times10^{15}$ $/m^3$. Thus the critical value $K_{CET} = 2.7\times10^{24}$ $K^{3.4}/m^{4.4}s$.

During the LPD processing conditions, the normal temperature gradient G_n ahead of solidification front can be expressed as

$$\left|\vec{G}_n\right| = \sqrt{\left|\vec{G}_x\right|^2 + \left|\vec{G}_y\right|^2 + \left|\vec{G}_z\right|^2} \tag{2}$$

where G_x, G_y and G_z are temperature gradient along X, Y and Z axis direction, and can be calculated from the

temperature field of mathematical model. The normal solidification velocity V_n ahead of solidification front is linked geometrically to the heat source travel speed V_b by the angle θ between the normal direction of the solidification interface and the travel direction of the heat source, as given by the following equation, as shown in Fig. 2:

$$\left|\vec{V}_n\right| = \left|\vec{V}_b\right| \cdot \cos\theta \tag{3}$$

Since the normal temperature gradient G_n and normal solidification velocity V_n are parallel with same direction, and laser scans along positive X axis direction which also is parallel to V_b, the angle θ can also be described as

$$\cos\theta = \frac{\left|\vec{G}_x\right|}{\left|\vec{G}_n\right|} \tag{4}$$

In the present analysis, it is assumed that the growth of dendrites is epitaxial from the substrate and the SX nature of the substrate is thus maintained after the LPD process. For the face-centered cubic (FCC) nickel-based superalloys, the six direction ((001)/[100], (00-1)/[100], (010)/[100], (0-10)/[100], (100)/[100], (-100)/[100]) are the preferred growth directions. In the case of epitaxial columnar dendritic crystal growth, due to the restriction of preferred crystallographic direction, the dendrite growth velocity is not always equal to the normal solidification velocity ahead of solidification front V_n. At a given location of the solidification interface, it is assumed that the growth direction of dendrite trunk, which is selected among the six possible (001)/[100] crystallographic orientations, is the one that owns the largest $|G_{hkl}|^{3.4}/|V_{hkl}|$ ((hkl)/[100] represents a specific crystallographic orientation) ratio. According to equation 1, the microstructure development in the molten pool is not only influenced by the value of $|G_{hkl}|^{3.4}/|V_{hkl}|$ ratio, but also is influenced by the critical value of K_{CET} that determines the formation of stray grain. When the largest $|G_{hkl}|^{3.4}/|V_{hkl}|$ ratio among six preferred crystallographic orientations is below the critical value of K_{CET}, equiaxed grain forms ahead of the solidification front and removes the epitaxial growth of columnar dendrite. The actual dendrite trunk growth velocity V_{hkl} of the dendrite tip and temperature gradient G_{hkl} along a specific crystallographic orientation (hkl)/[100] was derived by Rappaz et al.[30]

$$\left|\vec{V}_{hkl}\right| = \frac{\left|\vec{V}_n\right|}{\cos\psi_{hkl}} \tag{5}$$

$$\left|\vec{G}_{hkl}\right| = \left|\vec{G}_n\right|\cos\psi_{hkl} \tag{6}$$

where Ψ_{hkl} is the angle between the normal n of the molten pool boundary and the specific (hkl)/[100] crystallographic orientation.

3. Experimental Procedure

An Ytterbium fiber laser with maximum 1000 W power was used as the heat source. The laser generates a circular beam of minimum 0.6 mm in diameter at the focal zone with a near Gaussian intensity distribution. The LPD process is protected by coaxial argon shielding gas (purity of 99.99%) fed through the coaxial nozzle with a flow rate of 6 L/min. The powder of SX superalloy Rene N5 (a trademark of GE company) was used in this experiment as the deposit material. A DZ125 (a trademark of GE company) plate used this experiment was cut into specimen with (001)/[100] crystallographic orientation normal to the depositing surface of specimen. The substrate surface was ground with 300-grit SiC paper and cleaned by acetone and alcohol before laser deposition. Table 1 shows the processing parameters of verification experiments relative to the numerical simulation. The laser power, scanning speed and powder feeding rate are invariant in the simulation and experiment, which are 250 W, 10 mm/s and 3 g/min respectively. Samples were mounted, polished and etched using standard metallographic techniques for nickel-based superalloy. Optical microscopy was used for microstructure analysis in the study.

Table 1. Processing parameters.

Scanning method	Overlapping ratio (%)
X-direction	17
X-direction	33
X-direction	51
X-Y-direction	33

4. Results and discussion

Fig. 3 shows the temperature field and associated molten pool with overlapping 33%. As shown in Fig.3 (a), the distribution of temperature filed of first layer and second layer changes little when the process reaches thermodynamic equilibrium. This is because the height of two-layer deposit is small and the associated thermal conduction situation changes little. Part of previous track is heated by laser beam and the associated temperature exceeds fusion point. As shown in Fig. 3 (b), the adjacent part of previous track is remelted. Unlike the molten pool of first track, the following is asymmetry in transvers section. The raised previous track lifts up the toe edge of the molten pool of adjacent track. In the processing of second layer, the top part of previous layer is remelted instead of the substrate. At the top surface of adjacent zone, a deposition valley forms. Accordingly, a melting ridge forms at the bottom of adjacent zone.

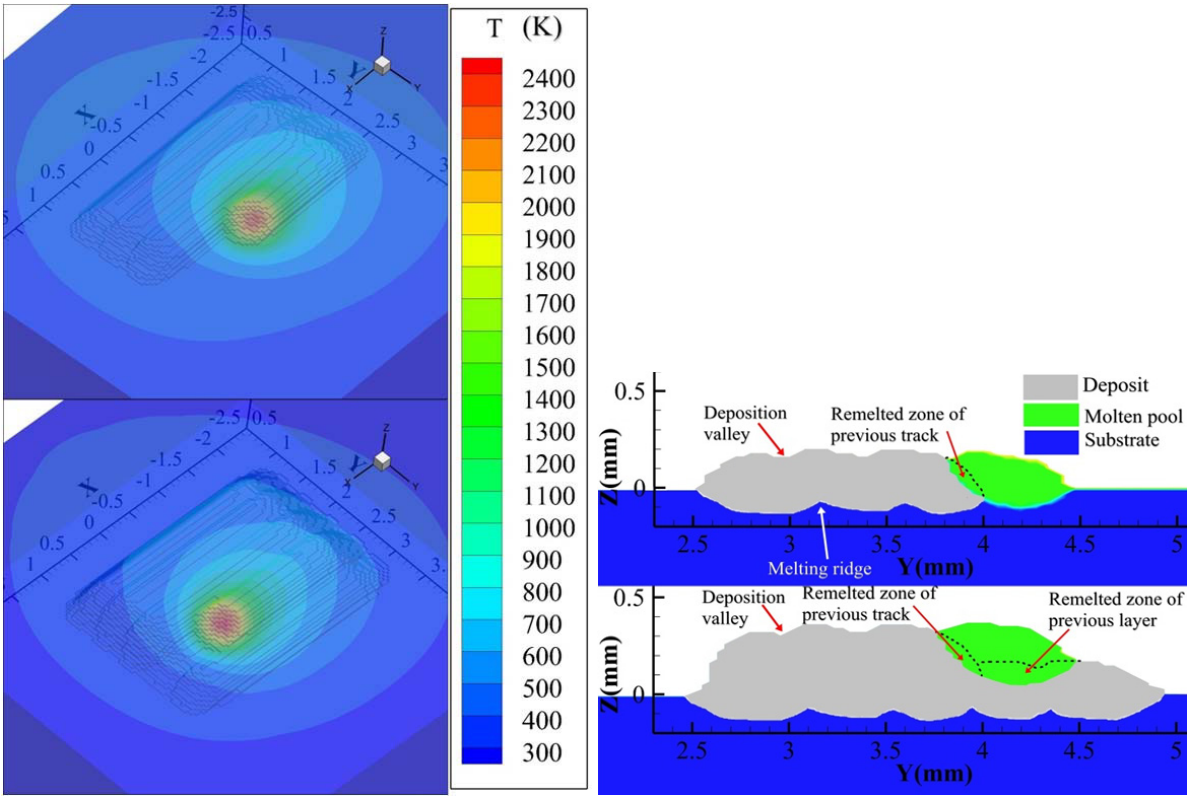

Fig. 3. The temperature field and associated molten pool.

Fig. 4 shows the variation of microstructure formation in multi-layer and multi-track LPD processing with the change of OR from 17% to 51%. As shown in Fig. 4(a), in the first track, (001)/[100] crystal grows epitaxially from

the substrate and is broke by the formation of stray grain. After the first track, due to the asymmetry of molten pool, the solidification conditions at the lifted toe changes and (010)/[100] preferred crystallographic orientation is active instead of (001)/[100] crystallographic orientation. Since the stray grain of previous track could not supply a fine epitaxial base for the remelted zone, crystal growth pattern at the lifted toe of molten pool is complex. Some crystal grows along (010)/[100] crystallographic orientation, nevertheless the growth direction of other crystals always is between (001)/[100] and (010)/[100] crystallographic orientations. In order to simplify the description of microstructure distribution, all these epitaxial crystals deviate from (001)/[100] crystallographic orientation at the lifted toe zone is defined as (010)/[100] crystal. Duing the processing of second deposited layer, the stray grain and (010)/[100] crystal of previous layer is remelted, which directly determines whether the (001)/[100] crystal can grows continuously or not. Usually, the melting ridge represents the minimum melting depth of the deposited layer, and corresponds to the (010)/[100]crystal zone of previous layer. When the OR is 17%, the deposition valley is very low, and the (010)/[100] crystal forms near the melting ridge. The melting ridge of above layer is too large to support enough to melting depth to remelt all (010)/[100] crystal and stray grain of previous layer. Thus some stray grain and (010)/[100] crystal are residual. When the OR is 33%, the smaller deposition valley makes that the top surface is more smooth than that of OR=17% and the of (010)/[100] crystal appears near the top surface. Smaller melting ridge increases the minimum melting depth. Thus all stray grain and (010)/[100] crystal are remelted. The continuity and consistency of the epitaxial columnar dendrite is better than that of 17%. When the OR is 51%, there are smallest deposition valley and melting ridge. Unlike the OR=17% or 33%, the height of deposited layer is far greater than that of single track. The formation of stray grain and (010)/[100] crystal is enhanced. Especially, the area of (010)/[100] crystal expands with the increase of inclination of solid/liquid interface near the toe zone. Due to the large OR, more layers are needed to reach the steady state of molten pool relative to OR =17% and 33%, and the geometry of molten pools near deposit edges changes sharply. The two edges become slopes, which affect the molten pool geometry and associated microstructure of the above tracks. The melting bottom of above layers does not keep in horizontal line. The tracks in middle have smaller melting depth than that of tracks at edges. Thus Some stray grain and (010)/[100] crystal are residual, as shown in Fig. 4(c). With the increase of depositing layers, the accumulation effect of inclined deposit edge will lead to defect such as residual stray grain at the edges.

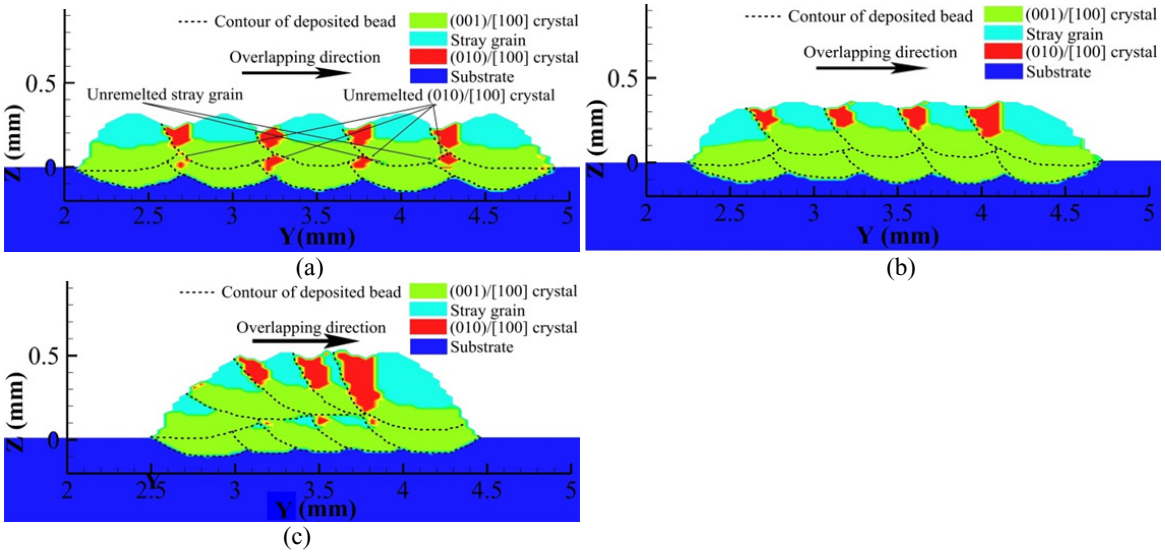

Fig. 4. The variation of microstructure in X-direction deposit with the change of OR = (a) 17%; (b) 33% and (c) 51%.

Fig. 5 shows the microstructure in X-Y-direction deposit with OR=33%. There are no residual stray grain and (010)/[100] crystals. (010)/[100] crystal grows continuously in the deposit. The molten pool of the second deposited layer keeps stable and the edges of deposit are near to steep, which benefits more layer deposition without defects formed at the edge of deposit. Thus, comparing the Fig. 4(b) and Fig. 5, one can find that X-Y-direction scanning

method is more stable than X-direction to keep the continuity and consistency of epitaxial growth in multi-layer and multi-track deposit.

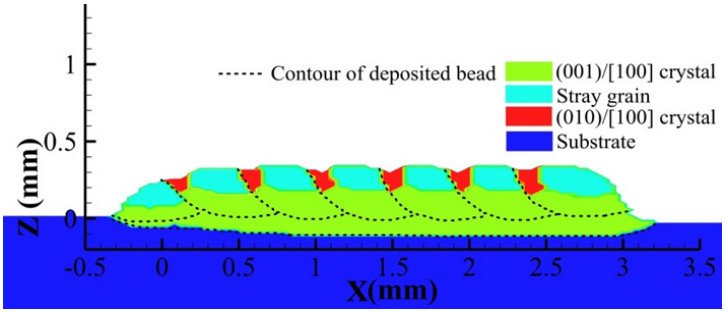

Fig. 5. The microstructure in X-Ydirection deposit with OR = 33%.

5. Experimental verification

Figure 6 shows the microstructure of double-layer and three-track LPD processing with OR=51%. The (001)/[100] crystal grows epitaxially from the substrate, and is replaced by the formation of stray grain. At the lifted toe of deposited track, (010)/[100] crystal forms. Near the melting ridge of first layer, the columnar dendrite can grow epitaxially on the base of the previous epitaxial columnar dendrite. The melting depth of the above deposited layer is not equilibrium relative to the first deposited layer. Some stray grains in first layer are residual due to the deficiency of melting depth of the above layer. The first and third tracks in the above layer incline sharply, and the outer toe edge has enough melting depth to ensure the continuous growth of epitaxial columnar dendrite. Nevertheless the second track in the above layer has lowest melting depth at the melting ridge, and some (010)/[100] crystal is unremelted. A crack forms in the epitaxial growth from stray-grain base and propagate into the third track of above layer.

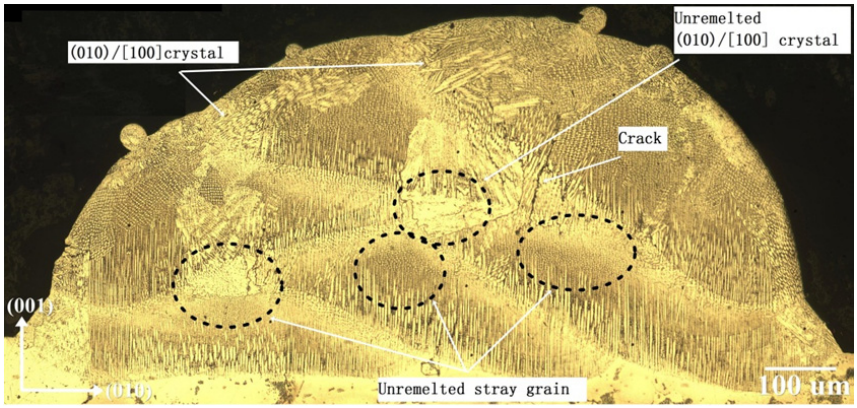

Fig. 6. The microstructure in deposit with OR = 51%.

According to the discussion results, a four-layer deposit between simulation and experiment are compared. In order to reduce the concentration of thermal stress in deposit, the scanning method is designed as shown in Fig. 7 (a). Comparing the Fig. 7 (a) and 7 (b), it is obvious that the epitaxial columnar dendrite can growth continuously and consistently in multi-layer and multi-track of LPD processing.

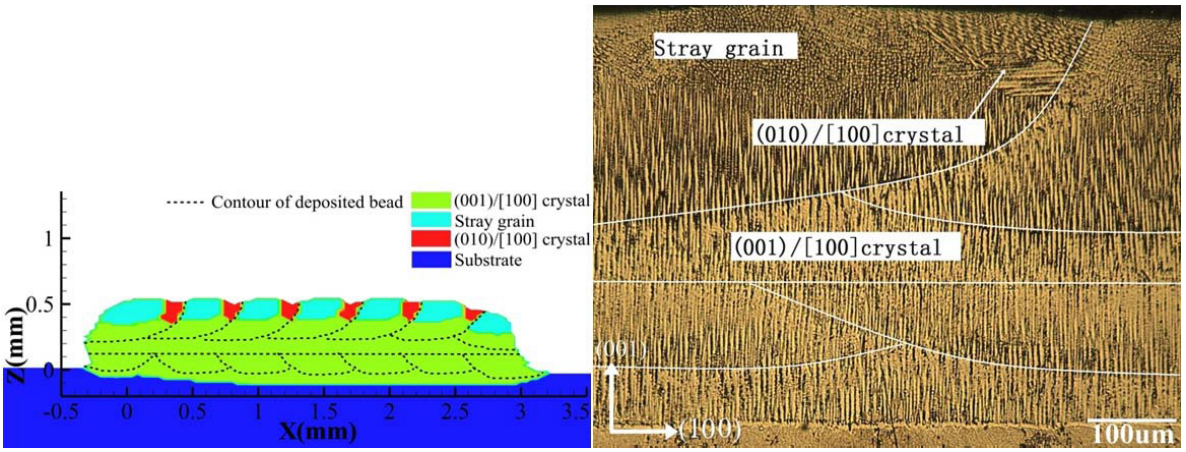

Fig. 7. The microstructure in X and Y-direction deposit with OR= 33%.

6. Conclusion

In this study, a 3D mathematical model was developed to simulate the crystal growth and microstructure formations during a LPD of SX superalloy. The simulation and experimental results agree well. The OR has a predominant effect on the crystal growth and microstructure formation in deposit. Small or large OR can cause residual stray grain and (010)/[100] crystal. A proper OR can smooth the deposit layer and achieve the continuous epitaxial growth in deposit. X-Y-direction scanning method can reduce the effect of variation of molten pool shape to the crystal growth and can ensure the continuity and consistency of epitaxial columnar dendrite in deposit.

Acknowledgements

This work was supported by the National Natural Science Foundation of China (Grant No. 51175338) and Pujiang Talent Program (Grant No. 12PJ1404400). The authors would also like to thank Yanming Li, Henry Peng from GE Global Research Shanghai for their support in acquiring materials and assistance in obtaining the experimental results.

References

[1] S. Babu, S. David, J. Park, J. Vitek, *Science and Technology of Welding & Joining* 2004, vol. 9, pp. 1-12.
[2] S. David, J. Vitek, S. Babu, L. Boatner, R. Reed, *Science and Technology of Welding & Joining* 1997, vol. 2, pp. 79-88.
[3] W. Schlachter, G. Gessinger, *E. Bachelet et al* 1990, p. 1.
[4] M. Gäumann, C. Bezencon, P. Canalis, W. Kurz, *Acta materialia* 2001, vol. 49, pp. 1051-1062.
[5] J. Choi, B. Dutta, J. Mazumder, DTIC Document, 2009.
[6] J. Milewski, G. Lewis, D. Thoma, G. Keel, R. Nemec, R. Reinert, *Journal of Materials Processing Technology* 1998, vol. 75, pp. 165-172.
[7] M. Gremaud, I.-D. Wagnière, A. Zryd, W. Kurz, *Surface Engineering* 1996, vol. 12, pp. 251-259.
[8] M. Gäumann, S. Henry, F. Cleton, J.D. Wagniere, W. Kurz, *Materials Science and Engineering: A* 1999, vol. 271, pp. 232-241.
[9] X. Do, D. Li, A. Zhang, B. He, H. Zhang, T. Doan, *Journal of Laser Applications* 2013, vol. 25, p. 012007.
[10] J. Hunt, *Materials Science and Engineering* 1984, vol. 65, pp. 75-83.
[11] M. Rappaz, S. David, J. Vitek, L. Boatner, *Metallurgical Transactions A* 1990, vol. 21, pp. 1767-1782.
[12] M. Rappaz, S. David, J. Vitek, L. Boatner, *Metallurgical Transactions A* 1989, vol. 20, pp. 1125-1138.
[13] W. Liu, J. DuPont, *Acta materialia* 2004, vol. 52, pp. 4833-4847.
[14] W. Liu, J. DuPont, *Acta materialia* 2005, vol. 53, pp. 1545-1558.
[15] T. Anderson, J. DuPont, T. DebRoy, *Acta Materialia* 2010, vol. 58, pp. 1441-1454.
[16] L. FENG, W. HUANG, X. Lin, H. YANG, Y. LI, J. Yang, *Chinese Journal of aeronautics* 2002, vol. 15, pp. 121-127.
[17] S. Yang, W. Huang, W. Liu, M. Zhong, Y. Zhou, *Acta materialia* 2002, vol. 50, pp. 315-325.
[18] E. Toyserkani, A. Khajepour, S. Corbin, *Journal of Laser Applications* 2003, vol. 15, p. 153.
[19] E. Toyserkani, A. Khajepour, S. Corbin, *Optics and Lasers in Engineering* 2004, vol. 41, pp. 849-867.
[20] H. Qi, J. Mazumder, H. Ki, *Journal of applied physics* 2006, vol. 100, pp. 024903-024903-024911.
[21] He.X, Mazumder.J, *Journal of Applied Physics* 2007, vol. 101, p. 9.

[22] X. He, L. Song, G. Yu, J. Mazumder, *Applied Surface Science* 2011.
[23] S. Wen, Y.C. Shin, *Journal of Applied Physics* 2010, vol. 108, pp. 044908-044908-044909.
[24] L. Han, K. Phatak, F. Liou, *Metallurgical and Materials Transactions B* 2004, vol. 35, pp. 1139-1150.
[25] L. Han, K.M. Phatak, F. Liou, *Journal of Laser Applications* 2005, vol. 17, p. 89.
[26] Peyre.P, Aubry.P, Fabbro.P, Neveu.P, Longuet.A, *Journal Applied of Physicals* 2008, vol. 41, p. 10.
[27] Z. Liu, H. Qi, *Metallurgical and Materials Transactions A*, pp. 1-13.
[28] J. Vitek, *Acta materialia* 2005, vol. 53, pp. 53-67.
[29] J. Liu, L. Li, *Optics & Laser Technology* 2005, vol. 37, pp. 287-292.
[30] M. Rappaz, *International Materials Reviews* 1989, vol. 34, pp. 93-124.